JOURNAL OF GUIDANCE, CONTROL, AND DYNAMICS
Vol. 21, No. 2, March–April 1998

Classically Rationalized Low-Order, Robust Structural Controllers

Mark E. Campbell* and Edward F. Crawley†
Massachusetts Institute of Technology, Cambridge, Massachusetts 02139

An experimental and analytical comparison of classically rationalized and optimal control design techniques is conducted. Classically rationalized compensators blend the loop assignments, complex topological design, and robustness of optimal controllers and the lower order, robustness, and practical insight of classical controllers. The single-input/single-output disturbance rejection problem for controlled structures is divided into four distinct topologies, and optimal controllers are designed and interpreted classically. The observations are then summarized into a set of design rules for the design of low-order robust controllers. Classically rationalized and robust compensators are experimentally implemented on the Middeck Active Control Experiment, a Shuttle flight experiment that flew on STS-67 in March 1995.

I. Introduction

WITH the evolution of controlled structures, a control design methodology is required that delivers required performance with minimum compensator size and maximum robustness. The literature of the past decade is replete with optimal solutions to this problem, but few shed practical insight into the philosophy embedded within them or the relationship to classical approaches. The best solutions address the three main issues in controlled structures: robustness, order, and topological complexity [multi-input/multi-output (MIMO), noncollocated, etc.].

Models of lightly damped structures can be extremely sensitive to errors, so that small parameter variations can lead to large variations in the frequency response. The resulting closed-loop stability concerns pose robustness problems for the control designer. There are many control design methodologies that can be used to increase robustness to parametric uncertainty.[1–3] In only a few cases,[2,4] however, are practical issues addressed such as which modes must be robustified and how and why the compensator actually adds robustness.

Lightly damped structures tend to have many significant modes within the working frequency range. Therefore, mathematical models of these systems are very large. Many optimal compensation techniques, however, create controllers equal to or larger than that of the mathematical model. Compensator truncation techniques have been developed that provide a ranking of the important dynamics.[5,6] These methods, however, do not provide physical insight into the actual number of states to retain or which states are essential to the robust stability and performance. Maximum entropy/optimal projection[2] is one of the only techniques that addresses both robustness and order directly in the design process.

As the controlled structures field matures, the complexity of topologies increases dramatically. The addition of numerous inputs, outputs, performances, and disturbances provides a great challenge to the control designer in the areas of MIMO control, actuator–sensor placement, and input–output pair choices for minimizing a given disturbance-performance metric. In general, compensator design techniques that work with state-space equations can handle the MIMO control problem but not constrained topologies. Although constrained topology design methods have been proposed,[7] insight into actuator–sensor placement and input–output pairing for minimizing a specific performance objective is absent.

The objective of this work is to thoroughly examine typical optimal approaches for their benefits and drawbacks in the areas of order, robustness, and topological complexity. The advantages of these controllers are then used to develop a set of classical design rules for the design of low-order, robust controllers for structures. The control methodology, termed classically rationalized controllers, addresses the following issues: which modes need to be robustified, how to add robustness, which dynamics are superfluous in robust designs, and actuator–sensor selection for performance improvement.

Because structural systems can be so complex that insight into controller interpretation is easily lost, a few simplifying assumptions are made. First, the systems analyzed contain a scalar disturbance, performance, input, and output. Although this assumption is quite restrictive, the ultimate design rules address multivariable design using a sequential loop closure method. Second, the input and output are collocated. This is also quite restrictive, but because the disturbance and performance can be noncollocated, the rules are still quite general.

This work complements and contrasts with that of Wie and Byun[8] and Wie et al.,[9] who developed a control design strategy based directly on classical concepts. The design rules developed in this work add two enhancements. First, the topologies examined are more general by not restricting the disturbance to enter only at the plant input or the performance to be the measured plant output and by addressing MIMO designs. Second, each rule is motivated by insight developed from the examination of the structure of optimal compensators, not classical design itself. Although a subset of the design rules may be similar, the motivation and process of creating the design rules for the two approaches are distinct.

A preliminary discussion of topics including structural control topologies and regions of control functionality is given. Next, the linear quadratic Gaussian (LQG) compensator[10] is introduced because of its ability to handle complex topologies. In addition, the asymptotic properties of the single-input/single-output (SISO) LQG compensator are presented to clearly show the function of the compensator in particular frequency ranges. For a low-order sample problem, LQG and frequency robust sensitivity weighted (SW) LQG[11,12] controllers are designed and examined. This simple example demonstrates order, robustness, and topological complexity issues present in many practical problems, thereby motivating the classically rationalized design rules. Finally, the classically rationalized design rules are used to design and experimentally implement low-order, robust controllers in 1 and 0 g for the Middeck Active Control Experiment (MACE), a Shuttle flight experiment that flew on STS-67 in March 1995 (Refs. 13 and 14).

II. Structural Control Problem

In the structural control problem, two primary issues give guidance and understanding to interpreting the compensator designs.

Presented as Paper 94-1564 at the AIAA/ASME/ASCE/AHS/ASC 35th Structures, Structural Dynamics, and Materials Conference, Hilton Head, SC, April 18–20, 1994; received April 26, 1996; revision received Feb. 20, 1997; accepted for publication July 30, 1997.

*Research Associate, Space Engineering Research Center; currently Assistant Professor, Department of Aeronautics and Astronautics, University of Washington, Box 352400, Seattle, WA 98195-2400. Member AIAA.

†Professor of Aeronautics and Astronautics and MacVicar Faculty Fellow and Director, Space Engineering Research Center. Fellow AIAA.

The first is the relationships (location and type) between the performances, outputs, inputs, and disturbances. The second issue is the frequency range in which a structural mode lies, with respect to the required performance metric. This establishes the level of control authority required for a particular mode.

A. SISO Structural Control Topologies

Consider a structural system with scalar disturbance w, input u, output y, and performance z:

$$\dot{x} = Ax + B_u u + B_w w, \qquad y = C_y x + v, \qquad z = C_z x \quad (1)$$

where $x \in \mathbb{R}^n$ and v is the sensor noise. In transfer function form,

$$\begin{bmatrix} z \\ y \end{bmatrix} = G(s) \begin{bmatrix} w \\ u \end{bmatrix} = \begin{bmatrix} g_{zw} & g_{zu} \\ g_{yw} & g_{yu} \end{bmatrix} \begin{bmatrix} w \\ u \end{bmatrix} = \begin{bmatrix} \dfrac{n_{zw}}{d} & \dfrac{n_{zu}}{d} \\ \dfrac{n_{yw}}{d} & \dfrac{n_{yu}}{d} \end{bmatrix} \begin{bmatrix} w \\ u \end{bmatrix} \quad (2)$$

Examination of the 2×2 matrix $G(s)$ gives rise to four structural control topologies.

1) An input analogous topology is when the disturbance w and input u are analogs or enter into the system in an identical manner, i.e., $B_w = B_u$ and

$$G_{\mathrm{IA}} = \begin{bmatrix} g_{zu} & g_{zu} \\ g_{yu} & g_{yu} \end{bmatrix}$$

2) An output analogous topology is when the performance z and output y are analogs or enter into the system in a similar or analogous manner and

$$G_{\mathrm{OA}} = \begin{bmatrix} \phi_{zy} g_{yw} & \phi_{zy} g_{yu} \\ g_{yw} & g_{yu} \end{bmatrix}$$

3) A fully analogous topology is when both the disturbance w and input u are analogs, the performance z and output y are analogs, and

$$G_{\mathrm{FA}} = \begin{bmatrix} \phi_{zy} g_{yu} & \phi_{zy} g_{yu} \\ g_{yu} & g_{yu} \end{bmatrix}$$

4) A nonanalogous topology is when there is no specific relationship between the disturbance w and input u or between the performance z and output y and

$$G_{\mathrm{NA}} = \begin{bmatrix} g_{zw} & g_{zu} \\ g_{yw} & g_{yu} \end{bmatrix}$$

Note that, in these definitions, $\phi_{zy}(s)$ is a stable, minimum-phase function used to allow the performance z to be a derivative, integral, or frequency shape of the output y.

B. Regions of Control Functionality

The frequency spectrum of a structural control system can be divided into four regions, depending on the type of compensation needed and the closed-loop performance objective. Figure 1 shows typical loop and closed-loop transfer functions. In addition, the concept of a dereverberant transfer function is introduced. The response at any point on a structure can be considered to be the sum of two parts: a direct field due to local dynamics and a reverberant field caused by the energy reflected back from other parts of the structure. The term dereverberant implies that the reverberant part of the response has been removed. Therefore, the dereverberant portion of the transfer function is the backbone, whereas the reverberant portion creates the lightly damped poles and zeros. The dereverberant transfer function can be approximated by drawing a smooth curve through the backbone.

Regions 1 and 2 are defined by the performance objective or disturbance rejection requirement. In region 1, the closed-loop system requires the open loop g_{zw} dereverberant transfer function to be lowered to meet the performance specification, as shown in Fig. 1b.

In regions 2 and 3, primarily rate feedback is needed, with the division between the two regions the crossover of the dereverberant loop transfer function. Motivation for this rate feedback, however, is the performance objective in region 2, whereas it is stability in region 3. In region 2, the open-loop dereverberant g_{zw} meets the performance specification, but the reverberant g_{zw} does not, as shown in Fig. 1b. The loop gain is greater than unity, and all modes are phase stabilized. In region 3, the dereverberant loop transfer function has crossed over, but at some frequencies, the reverberant loop transfer function may exceed unity, as shown in Fig. 1a. These modes may need to be gain stabilized, depending on the phase of the loop transfer function.

Unlike the modes in region 3, all of the structural modes in region 4 are gain stabilized, due to the rolloff of the reverberant loop transfer function. Therefore, in region 4 no additional compensation is needed. The division of the frequency spectrum of these four regions will aid in the understanding of the structure of the optimal compensators.

III. Control Design Methods

There are many types of control design methodologies that could be used to gain insight and to develop classically rationalized design rules. In this section, two methods are presented because of their simple application to controlled structures: the LQG method and frequency robust SWLQG.

A. LQG Controllers

LQG compensators[10] are $\mathcal{H}_2$ optimal compensators designed by solving two separate but dual problems: the linear quadratic regulator (LQR) and Kalman filter. The LQR problem minimizes a quadratic cost on the states and inputs:

$$J_{\mathrm{LQR}} = \int_0^\infty \left(x^T C_z^T C_z x + \rho u^T u \right) \mathrm{d}t \quad (3)$$

where ρ is a positive scalar and yields a matrix of optimal gains F for state feedback.

The Kalman filter minimizes the state estimation error where the disturbance and sensor noise are assumed to be zero mean, Gaussian processes that are uncorrelated in time. The Kalman filter in this work utilizes the following covariances:

$$E\{ww^T\} = I, \qquad E\{vv^T\} = \theta \cdot I > 0 \quad (4)$$

where θ is a positive scalar and yields a matrix of optimal gains H for state estimation.

Combining the state feedback and estimation problems, the LQG compensator is given by

$$K_{\mathrm{LQG}}(s) = F(sI - A + B_u F + HC_y)^{-1} H \quad (5)$$

B. LQG Asymptotes

In many cases, the low- and high-frequency regions of SISO LQG controllers can be represented using a set of asymptotes. These asymptotes are formed by allowing the LQG parameters ρ and θ to vary from 0 to ∞. The SISO LQG asymptotes are, therefore, introduced here to more fully understand the structure of the compensators in particular frequency ranges for each of the SISO structural control topologies given in Sec. II.A. The derivation of asymptotes is given in Ref. 15 and summarized here. Note that the transfer functions g_{yw} and g_{zu} are assumed to be minimum phase.

The SISO low-gain LQG asymptote represents the LQG controller at high frequency and is found using the expensive control LQR asymptote ($\rho \gg 0$) and the low-noise Kalman filter asymptote ($\theta \ll 0$):

$$K_{\mathrm{LG}}(s) = \lim_{\substack{\theta \to 0 \\ \rho \to \infty}} K(s)$$

$$= F_{\dot{q}1} b_{w1} \left[s \prod_{i=2}^{n} \left(s^2 + 2\zeta_i \omega_i s + \omega_i^2 \right) \Big/ n_{yw} \right] = F_{\dot{q}1} b_{w1} \frac{s\tilde{d}}{n_{yw}} \quad (6)$$

where ω_i and ζ_i refer to the ith frequency and damping ratio, $F_{\dot{q}i}$ and b_{wi} refer to the LQR gain and ith velocity state of B_w, and n_{yw} is the numerator of the disturbance-output transfer function. Also, the modes have been ordered such that the first mode is the most

controllable/observable (largest residue), and $\tilde{d}$ is the denominator except for this mode.

The SISO high-gain LQG asymptote represents the LQG controller at low frequency and is found using the cheap control LQR ($\rho \ll 0$) and low-noise Kalman filter ($\theta \ll 0$) asymptotes and assuming the estimator is faster than the regulator, or $\theta \ll \rho$:

$$K_{\mathrm{HG}}(s) = \lim_{\substack{\theta \to 0 \\ \rho \to 0}} K(s) = \frac{g_{zw}}{\pm\sqrt{\rho} g_{yw} + (g_{zu} g_{yw} - g_{zw} g_{yu})} \tag{7}$$

The assumption $\theta \ll \rho$ is made to examine a smaller subset of controllers. Relaxing this assumption would add $\pm\sqrt{\theta} g_{zu}$ to the denominator of this asymptote.

Table 1 shows the SISO low- and high-gain LQG asymptotes, as defined by Eqs. (6) and (7), simplified for each of the SISO structural control topologies. The low-gain asymptote (high-frequency LQG)

Table 1 Low- and high-gain LQG asymptotes for each structural control topology

Topology	$K_{\mathrm{LG}}(s) = \lim_{\substack{\theta \to 0 \\ \rho \to \infty}} K_{\mathrm{LQG}}(s)$	$K_{\mathrm{HG}}(s) = \lim_{\substack{\theta \to 0 \\ \rho \to 0}} K_{\mathrm{LQG}}(s)$
Fully analogous	$F_{\dot{q}1} b_{u1} \dfrac{s\tilde{d}}{n_{yu}}$	$\dfrac{\pm 1}{\sqrt{\rho}} \dfrac{\phi_{zy} n_{yu}}{n_{yu}}$
Output analogous	$F_{\dot{q}1} b_{w1} \dfrac{s\tilde{d}}{n_{yw}}$	$\dfrac{\pm 1}{\sqrt{\rho}} \dfrac{\phi_{zy} n_{yw}}{n_{yw}}$
Input analogous	$F_{\dot{q}1} b_{u1} \dfrac{s\tilde{d}}{n_{yu}}$	$\dfrac{\pm 1}{\sqrt{\rho}} \dfrac{n_{zu}}{n_{yu}}$
Nonanalogous	$F_{\dot{q}1} b_{w1} \dfrac{s\tilde{d}}{n_{yw}}$	$\dfrac{-g_{zw}}{g_{zw} g_{yu} - g_{zu} g_{yw}}$

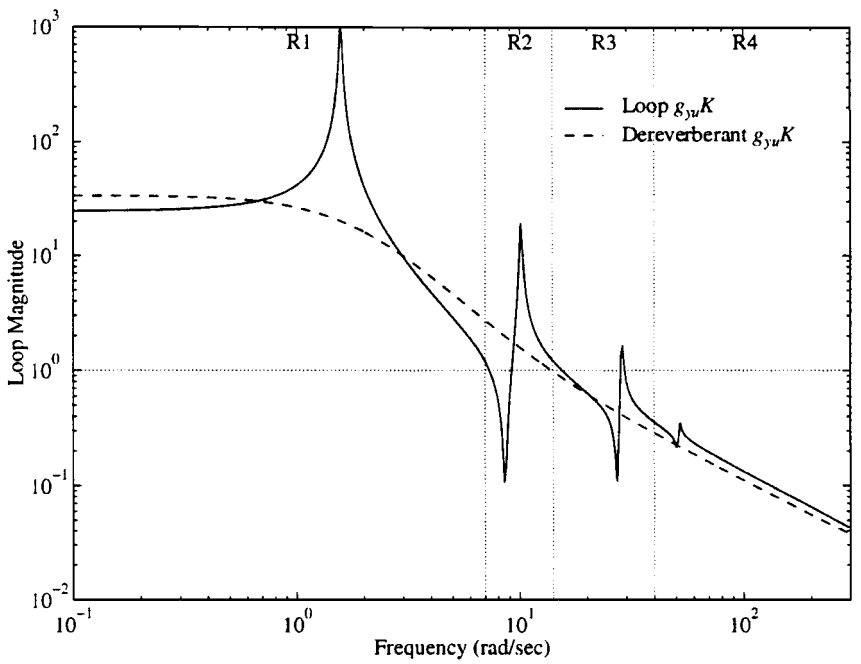

a) Loop transfer function $g_{yu}K$

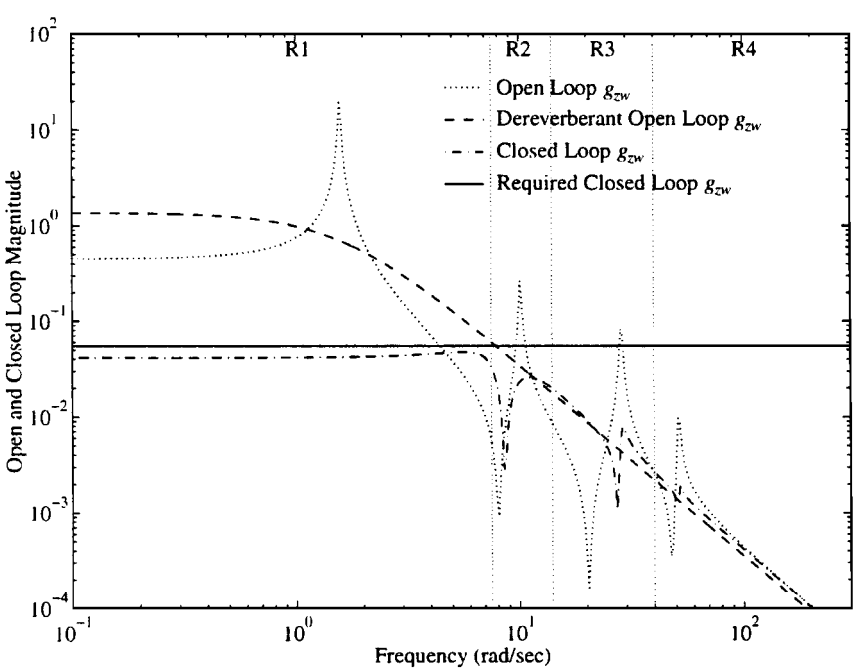

b) Open- and closed-loop g_{zw} transfer functions (the required closed-loop performance specification is achieved)

Fig. 1 Typical SISO structural control system.

is a low-gain, rate feedback inversion of the disturbance-output transfer function, except for the most controllable/disturbable mode. Therefore, in addition to the obvious influences of the g_{yu} (stability) and g_{zw} (performance) transfer functions, linear quadratic control design is also heavily influenced by the g_{yw} and g_{zu} transfer functions.

The high-gain asymptote is more easily understood by examining the closed-loop disturbance to performance transfer function for a given compensator $u = -Ky$:

$$(g_{zw})_{\mathrm{CL}} = \frac{g_{zw} + (g_{zw}g_{yu} - g_{zu}g_{yw})K}{1 + g_{yu}K} \tag{8}$$

The term $(g_{zw}g_{yu} - g_{zu}g_{yw})$ is the determinant of $G(s)$. If this determinant is 0, as in the input, output, and fully analogous cases, the asymptote (low-frequency LQG) achieves performance using very high gain. In addition, the pole-zero structure of the asymptote can be found using the zeros of the system. If the determinant of $G(s)$ is large, as in the nonanalogous case, the asymptote is a constant and achieves performance by creating a subtraction in the numerator of the closed-loop disturbance to performance transfer function.

C. SWLQG

SWLQG controllers[11,12] desensitize the LQG controller to variations in modal frequency. This is accomplished by changing the LQR and Kalman filter weighting matrices. For instance, in the SWLQR problem, the sensitized cost is

$$J_{\mathrm{SWLQR}} = \int_0^\infty \left(x^T C_z^T C_z x + \frac{\partial x^T}{\partial \alpha} R_{\alpha\alpha} \frac{\partial x}{\partial \alpha} + \rho u^T u \right) \mathrm{d}t \tag{9}$$

where α is the uncertain parameter. There is a dual change in the Kalman filter problem. It is noted that this robust control design method, although simple, is performed quickly and is adequate in designing controllers for a complex flexible structure such as MACE.[4]

IV. Sample Problem

To demonstrate and understand how the LQG and SWLQG controllers compensate a structural system, a small-order example is used. Although extrapolation to more practical systems may seem difficult, this simple example more clearly demonstrates many of the order, robustness, and complexity issues present in practical problems, thereby motivating the classically rationalized design rules. Figure 2 shows the four structural control topologies for the sample problem, where the performance is a linear position and the output is a linear velocity; the disturbance and actuator are linear forces on the masses. A summary of LQG and SWLQG controllers designed for each case is given here.

A. LQG Controllers

Figure 2a shows an example of a fully analogous control problem, where the performance z_1, output y_1, disturbance w_1, and input u_1 all act on the tip mass. The relation between z_1 (position) and y_1 (velocity) is an integrator [$\phi_{zy}(s) = 1/s$].

Figure 3 shows an eight-state LQG compensator for low noise and intermediate LQR control, along with the low- and high-gain LQG asymptotes defined for this topology and four regions of control. Notice how well the LQG compensator can be represented by its asymptotes. In region 1, the LQG compensator is a high-gain integrator, or uses position feedback, and matches the high-gain asymptote. In region 4, the compensator uses proportional or rate feedback, matching the low-gain LQG asymptote. A compensator zero changes the region 1 integral control to the region 4 proportional control, thus creating a proportional–integral (PI) controller.

The lightly damped open-loop mode at 10 rad/s in region 3 is interesting because the open-loop zero is exactly canceled by the compensator pole, but the open-loop pole is not exactly canceled by the compensator zero. This motivates a compensator pole-zero plot as a function of the LQR weighting ρ near the mode at 10 rad/s (Fig. 4). As ρ decreases, the gain increases and the mode being compensated shifts from region 4 to region 1. In region 4, the LQG controller cancels the open-loop, pole-zero pair with a compensator zero-pole pair. Although similar in region 3, the compensator zero does not completely cancel the open-loop pole, leaving a small residual pole-zero pair in the loop. In region 2, the compensator zero is close to the compensator pole, leaving a large residual pole-zero pair in the loop. In region 1, the LQG compensator contains a pole-zero cancellation, leaving the open-loop, pole-zero pair in the loop. The compensator pole does not move as a function of ρ. A summary of the LQG results (for each of the topologies) is given in Table 2.

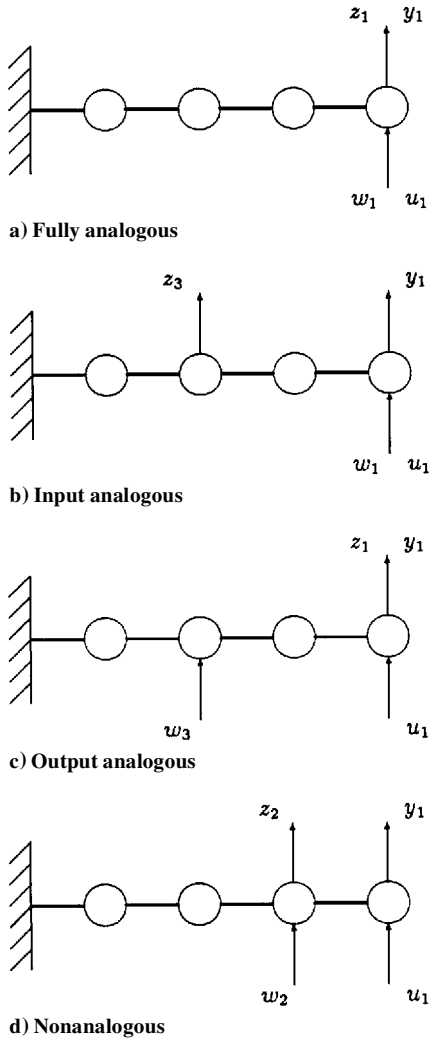

Fig. 2 Four structural control topologies on a four-mass cantilevered sample problem.

Figure 2b shows an example of an input analogous topology on the sample problem. Because the low-gain LQG asymptotes are the same (Table 1), regions 3 and 4 for the input and fully analogous controllers are identical. The high-gain LQG asymptotes are different, however, with the input analogous case being a high-gain filter, with poles and zeros n_{zu}/n_{yu}.

The output analogous problem in Fig. 2c is chosen because of its similarity to the input analogous example in Fig. 2b. For these two cases, the output y_1 and input u_1 and, therefore, input–output transfer functions g_{yu} are identical. In addition, even though the performance and disturbance are distinct (output analogous: z_1, w_3; input analogous: z_3, w_1), the disturbance-performance transfer functions g_{zw} are identical. The g_{yw} and g_{zu} transfer functions are the only differences between the two problems.

For a given compensator $u = -Ky$, the closed-loop disturbance-performance transfer function in Eq. (8) is identical for both the input and output analogous problems:

$$(g_{zw})_{\mathrm{CL}} = \frac{g_{zw}}{1 + g_{yu}K} \tag{10}$$

Given these similarities, intuitively the two cases should be compensated similarly.

Table 2 Summary of LQG compensators for SISO control topologies

Topology	Region 1	Region 2	Region 3	Region 4
Fully analogous	High gain $\phi_{zy}\frac{n_{yu}}{n_{yu}}$	Velocity feedback $\sim\phi_{zy}\frac{n_{yu}}{n_{yu}}$	Velocity feedback $\sim\frac{d}{n_{yu}}$	Low gain, rolloff $\frac{d}{n_{yu}}$
Input analogous	High gain $\frac{n_{zu}}{n_{yu}}$	Velocity feedback $\sim\frac{n_{zu}}{n_{yu}}$	Velocity feedback $\sim\frac{d}{n_{yu}}$	Low gain, rolloff $\frac{d}{n_{yu}}$
Output analogous	High gain $\phi_{zy}\frac{n_{yw}}{n_{yw}}$	Velocity feedback $\sim\phi_{zy}\frac{n_{yw}}{n_{yw}}$	Velocity feedback $\sim\frac{d}{n_{yw}}$	Low gain, rolloff $\frac{d}{n_{yw}}$
Nonanalogous	Constant gain $\frac{-g_{zw}}{g_{zw}g_{yu}-g_{zu}g_{yw}}$	Velocity feedback $\sim\frac{-g_{zw}}{g_{zw}g_{yu}-g_{zu}g_{yw}}$	Velocity feedback $\sim\frac{d}{n_{yw}}$	Low gain, rolloff $\frac{d}{n_{yw}}$

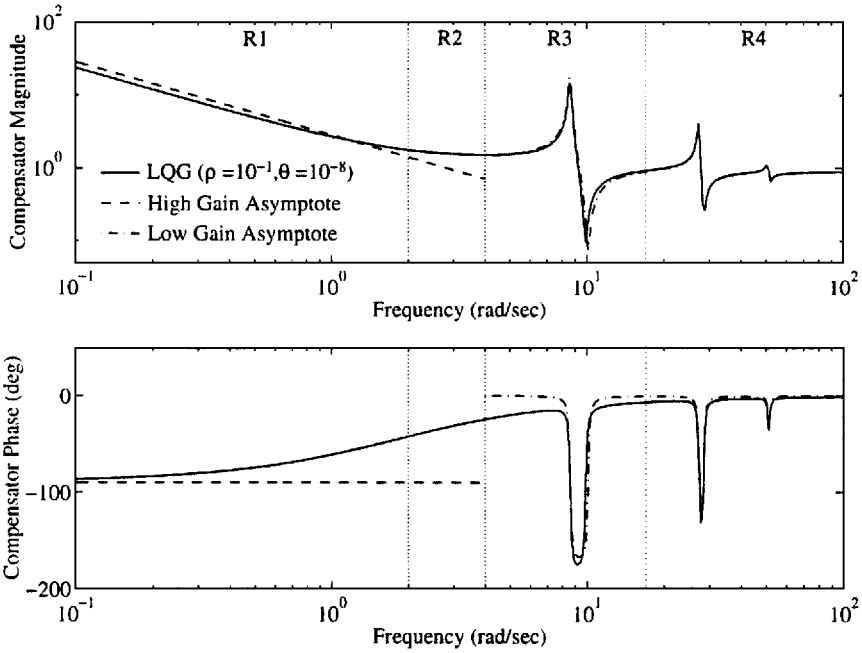

Fig. 3 LQG compensator K and the low- and high-gain LQG asymptotes for the fully analogous problem.

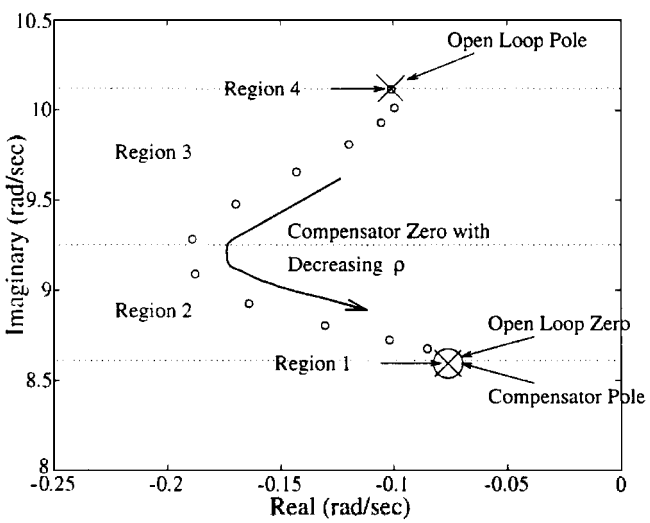

Fig. 4 Compensator pole-zero plot for changing ρ for the fully analogous problem.

The compensators for the input analogous topology are generally low bandwidth and stable primarily because g_{yw} is minimum phase. The compensators for the output analogous topology, however, are quite often unstable, nonminimum phase, and high bandwidth primarily because g_{yw} is nonminimum phase. If ρ is made small and θ is made large for the output analogous problem, the controllers become stable and minimum phase but still have a larger bandwidth than the input analogous controllers.

The nonanalogous topology is the most difficult to design and analyze. It is also the most common topology, however, often occurring in cases in which the control designer does not have influence on actuator–sensor placement. For this general topology, there are no simple explicit relationships among the system parameters z, y, w, and u.

Table 1 shows that the low-gain LQG asymptote for the nonanalogous topology is a function of g_{yw}, similar to the output analogous topology. Therefore, unstable, nonminimum-phase controllers quite often result. The high-gain LQG asymptote is a constant and attempts to minimize the closed-loop system by creating a subtraction in the closed-loop disturbance to performance transfer function [Eq. (8)].

B. SWLQG

Figure 5 shows a summary of the frequency robust SWLQG designs for the fully analogous problem given in Fig. 2a. Figure 5a shows three compensators with varying sensitivity to uncertainty in the frequency of the 10 rad/s mode in region 2. As the mode is desensitized, the weak open-loop pole and zero inversion by the LQG compensator becomes a compensator pole-zero cancellation. Figure 5b shows the desensitized mode in region 3, where the strong open-loop pole and zero inversion of the LQG compensator becomes a classical notch filter. In addition, this notch filter becomes wider and deeper for increased uncertainty; these aspects were also demonstrated in maximum entropy designs.[2]

Desensitizing modes in region 1 did not affect the compensator structure because it already contains pole-zero cancellations. In region 4, all modes are gain stabilized and, therefore, do not need to

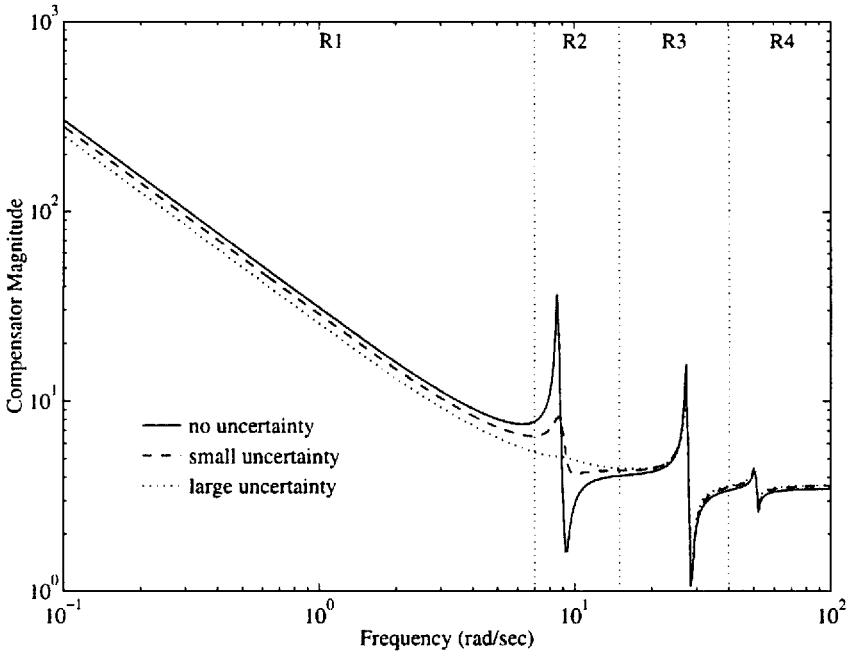

a) Three different uncertainties of a mode in region 2

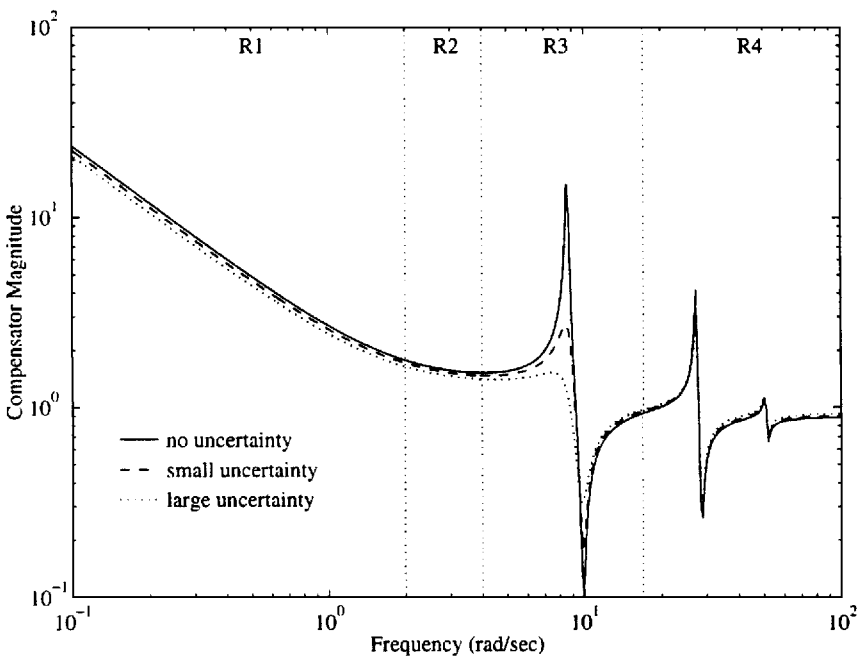

b) Three different uncertainties of a mode in region 3

Fig. 5 SWLQG controllers for the fully analogous example.

be robustified by definition. A summary of the SWLQG results (for each of the topologies) is given in Table 3.

Because of the similarities in regions 3 and 4 (low-gain asymptote) between the input and fully analogous examples, the SWLQG results are identical. In regions 1 and 2, however, desensitizing modes changed the input analogous controller from a filter n_{zu}/n_{yu} to velocity feedback with pole-zero cancellations n_{yu}/n_{yu}, depending on the level of robustness required.

SWLQG controllers designed for the output and nonanalogous examples were more difficult to interpret. The LQG controllers were primarily unstable and nonminimum phase, and robustifying usually reversed these characteristics. In region 3, the SWLQG controllers slightly changed the inversion of g_{yw} but did not always use notch filters as in the input and fully analogous cases. In regions 1 and 2, robustification usually led to a combination of the filter n_{zw}/n_{yu} and velocity feedback, depending on the level of robustness required.

In the nonanalogous topology, the velocity feedback of the SWLQG controller confirms that the subtraction in the numerator of the closed-loop, disturbance-performance transfer function [Eq. (8)] of the LQG controller is not robust because of practical limitations such as sensor noise and model uncertainty. Occasionally, the resulting controller uses high-gain control instead of velocity feedback with good performance results. This leads to a test of the ability of each y, u pair to minimize the closed-loop w to z transfer function using a high-gain compensator. Specifically, the magnitude of the disturbance to performance transfer function in region 1 is examined in open and closed loop (with a high-gain K):

$$\left| \frac{g_{zw}g_{yu} - g_{zu}g_{yw}}{g_{yu}} \right| \ll |g_{zw}| \tag{11}$$

The test is passed at all frequencies by the input–output pairs in the input, output, and fully analogous topologies. For the nonanalogous topology, however, typically only certain frequency ranges pass the test. If these frequency ranges are in region 1, where the controller obtains performance improvement, then the input–output pair is a

Table 3 Summary of SWLQG compensators for SISO control topologies

Topology	Region 1	Region 2	Region 3	Region 4
Fully analogous	High gain $\phi_{zy}\dfrac{n_{yu}}{n_{yu}}$	Velocity feedback $\phi_{zy}\dfrac{n_{yu}}{n_{yu}}$	Velocity feedback Notch	Low gain, rolloff $\dfrac{d}{n_{yu}}$
Input analogous	High gain $\sim\dfrac{n_{zu}}{n_{yu}}$	Velocity feedback $\dfrac{n_{yu}}{n_{yu}}$	Velocity feedback Notch	Low gain, rolloff $\dfrac{d}{n_{yu}}$
Output analogous	Velocity feedback $\sim\phi_{zy}\dfrac{n_{yw}}{n_{yw}}$	Velocity feedback $\sim\phi_{zy}\dfrac{n_{yw}}{n_{yw}}$	Velocity feedback $\sim\dfrac{d}{n_{yw}}$	Low gain, rolloff $\dfrac{d}{n_{yw}}$
Nonanalogous	Velocity feedback $\sim\dfrac{n_{zw}}{n_{yu}}$	Velocity feedback $\sim\dfrac{n_{zw}}{n_{yu}}$	Velocity feedback $\sim\dfrac{d}{n_{yw}}$	Low gain, rolloff $\dfrac{d}{n_{yw}}$

good choice for minimizing the closed-loop w to z transfer function. In frequency ranges where the test is not passed, closed-loop performance improvement is usually achieved by damping the open-loop system. Note that this test can also be used to select those sensor and actuator pairs that yield the best performance improvement.

V. Classically Rationalized Design Rules

Using only the beneficial aspects of the LQG and robust SWLQG controllers for the four structural control topologies in Tables 2 and 3, a set of classically rationalized design rules can now be developed. For these rules to be applicable to general problems, however, the issues of noncollocated input–output pairs and MIMO control are addressed first.

Collocated input–output pairs are used for simple, high-gain control because the transfer function contains alternating lightly damped poles and zeros.[16] When the input and output are noncollocated, however, the lightly damped zeros move such that there may be missing zeros and nonminimum-phase zeros between the poles. In the most common case where the input–output transfer function contains nonminimum-phase zeros, performance cannot be achieved in that frequency range. Therefore, in developing the classically rationalized design rules, only collocated input–output pairs are considered. Although this appears to limit the rules, much of the performance improvement of a multivariable controller is created by the inclusion of collocated loops. In addition, because the rules can be used to synthesize multivariable controllers with noncollocated disturbances and performances, there are numerous systems that would benefit from them, including a truss structure with active struts, a wing with piezoelectric patches, a rotor blade with local piezoelectric controllers, and a multiple-link robotic arm with actuators and sensors at the elbow.

Classical design has been used for many years because of its ease in design and implementation and inherent robustness. One method of constructing multivariable classical controllers is called sequential loop closure. A SISO classical controller is first designed around the highest-bandwidth loop and then closed analytically to create a new model. A controller is then designed using the next-lower-bandwidth loop of the new model, and so on. If the bandwidths are distinct, little interaction occurs between the controllers. Although this cannot be guaranteed, if collocated input–output pairs are used, an alternating pole-zero pattern results that is inherently robust to many types of controllers. If a sequential loop closure method is used with collocated input–output pairs and the stability and robustness of the final design is tested, the method actually works quite well even for similar bandwidths.

A. Procedure

The procedure for designing classically rationalized structural controllers is as follows.

1) Order loops highest to lowest bandwidth.
2) Design each loop with the following rules:
   a) region 1 rule: test input–output pair

$$\left|\frac{g_{zw}g_{yu}-g_{zu}g_{yw}}{g_{yu}}\right| \ll |g_{zw}|$$

   if test is passed, add dynamics n_{zw}/n_{yu} robustly, and if the test is not passed, use velocity feedback;
   b) region 2 rule: velocity feedback;
   c) region 3 rule: velocity feedback, notch filter robustly; and
   d) region 4 rule: rolloff, if g_{yu} contains rolloff dynamics, add lead.
3) Analytically close controller to get new open-loop plant.
4) Design controller for next-lower-bandwidth loop.
5) Analyze stability and robustness of multivariable controller.

B. Discussion

First, each of the loops to be closed is ordered from highest to lowest bandwidth for the sequential loop closure method. Controllers are then synthesized for each loop, based on the four frequency domain regions. By definition, robust performance is the primary concern in regions 1 and 2, whereas it is robust stability in regions 3 and 4.

In region 1, the ability of the input–output pair to use high-gain control is first tested according to Eq. (11). If the test is passed (all input, output, and fully analogous cases and a few nonanalogous cases), the region 1 rule is to use a robust filter n_{zw}/n_{yu} or matching this filter without sacrificing robustness. If the test is not passed (most nonanalogous cases), velocity feedback is used as motivated by the SWLQG controller in Table 3. Region 2 begins the transition to the concern of robust stability in regions 3 and 4. Therefore, the region 2 rule is a transition from region 1 control to velocity feedback, with no compensation of structural modes, as motivated by the SWLQG controllers (Fig. 5a).

The primary concern of region 3 is robust stability (g_{yu}) and because the input and fully analogous controllers were stable, minimum phase, and robust, these are used as a basis for the region 3 rule. As in Table 3 for these cases, the region 3 rule is velocity feedback with appropriately robust (wide and deep) notch filters where necessary. Region 4 contains only rolloff dynamics because all structural modes are gain stabilized. In most practical applications, however, there are heavily damped sensor/actuator dynamics. Therefore, the region 4 rule also adds lead to compensate for these dynamics.

Once the first controller has been designed, it is closed analytically around the open-loop plant, thus creating a new plant. The next-lower-bandwidth loop is then closed using this same procedure and so on until the complete multivariable controller has been synthesized. The final step is to analyze full multivariable controller for robustness and stability. This step checks the interaction of the loops, especially if they have similar bandwidths.

VI. Experimental Verification

Over 100 multivariable controllers were implemented in 1 and 0 g using the classically rationalized design rules on a variety of complex topologies. This section presents two of the more challenging topologies: a SISO nonanalogous topology and MIMO control using two disturbances and two performances. The controllers were all implemented on the MACE[13,14] (Fig. 6), a reusable dynamics and control laboratory designed to investigate issues associated with a change in operational environment of a flexible spacecraft from ground to space. Extensive modeling and control experiments were performed on the MACE during 14 days of on-orbit operations on STS-67 in March 1995 (Ref. 14).

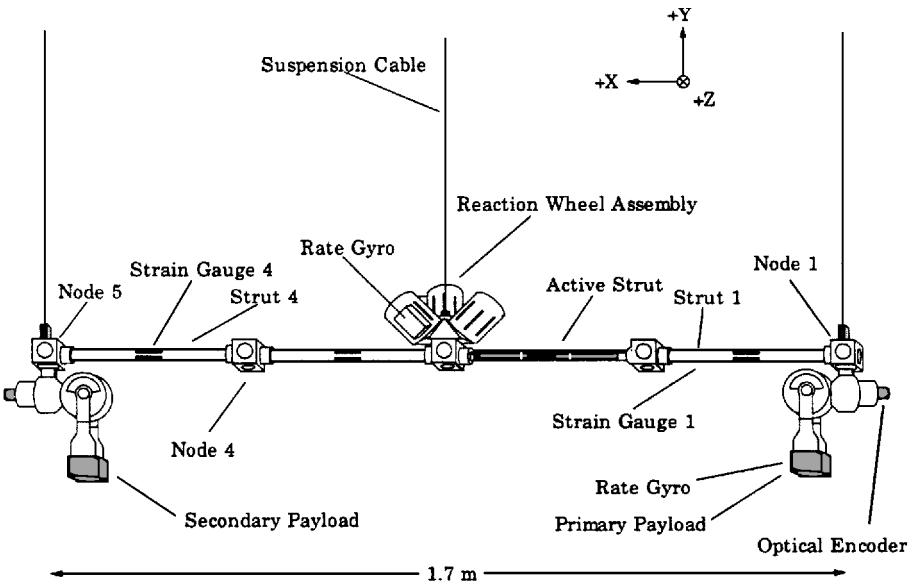

Fig. 6 MACE flight model.

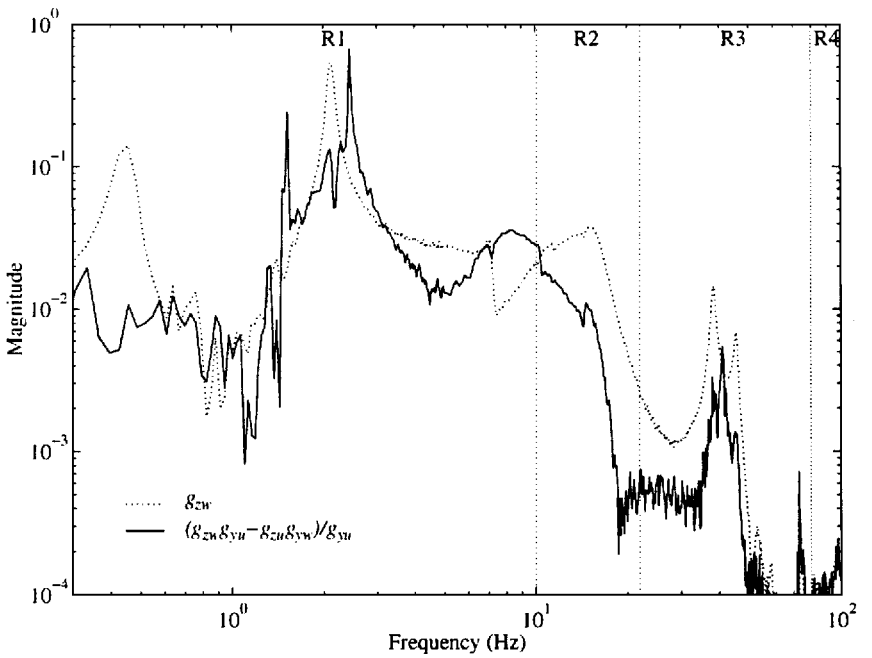

Fig. 7 Input–output test for the nonanalogous MACE 1-*g* experiment.

The specific control objective for the MACE was to reduce the inertial pointing error of the primary payload, while broadband disturbance(s) are applied to the secondary gimbal. A 1-*g* finite element model, consisting of 40 structural modes below 100 Hz, was created.[17] This model was appended with sensor dynamics, time delays, and amplifier gains and truncated to create a 100-state control design model. An analogous 80-state control design model for 0 *g* was created by removing the gravity and suspension effects from the 1-*g* model.[17]

The first controller shown is a SISO nonanalogous topology implemented on the MACE in 1 *g*. The performance z is the Z-axis integrated primary payload rate gyro, and the output y is the Z-axis bus rate gyro; the input u is the Z-axis bus reaction wheel, and disturbance w is broadband noise (0–50 Hz) entering the Z-axis secondary gimbal.

The first step in designing a classically rationalized controller is to test the input–output pair using Eq. (11). This is shown in Fig. 7. Interpreting the test, high-gain control achieves performance in the 10–50 Hz range but not in the 0–10 Hz range. This is especially true near the 2-Hz mode, where a high-gain controller would create a lightly damped resonance at 2.5 Hz. Therefore, the region 1 rule is velocity feedback. Regions 2 and 3 easily follow using velocity feedback and two notch filters to gain stabilize structural modes at 48 and 74 Hz, as shown in Fig. 8. The region 4 rule is a lead filter to counteract the rate gyro sensor rolloff. The synthesized classically rationalized controller shown in Fig. 8 contains eight states (two stabilized integrator, four notch filter, and two lead filter).

Figure 9 shows the measured closed-loop disturbance to performance transfer functions for the 8-state classically rationalized controller and a 48-state robust control design using the multiple model method.[1] Performance improvement of both compensators was quite similar, primarily achieved by damping the 2-Hz mode. In addition, the use of the actuator–sensor test to add insight into control design worked quite well by predicting that 1) the 2-Hz mode must be damped and 2) high-gain control can be used only in the 10–50 Hz range.

The second topology for which controllers were designed was a MIMO system for the MACE in 0 *g*, where the performance was a combination of the X and Z primary payload inertial pointing error, while broadband disturbances (0–50 Hz) are applied to two axes of the secondary gimbal. Note that these controllers were designed prior to the MACE flight, without the benefit of open-loop data for analysis, thus making the designs quite challenging.

Table 4 Summary of MACE 0-*g* classically rationalized MIMO controller

Loop	Sensor		Actuator	Type	States
1	*X*-axis bus rate gyro	→	*X*-axis reaction wheel	Nonanalogous	6
2	*Y*-axis bus rate gyro	→	*Y*-axis reaction wheel	Nonanalogous	6
3	*Z*-axis bus rate gyro	→	*Z*-axis reaction wheel	Nonanalogous	8
4	*X*-axis primary rate gyro	→	*X*-axis primary gimbal	Output analogous	10
5	*Z*-axis primary rate gyro	→	*Z*-axis primary gimbal	Output analogous	10

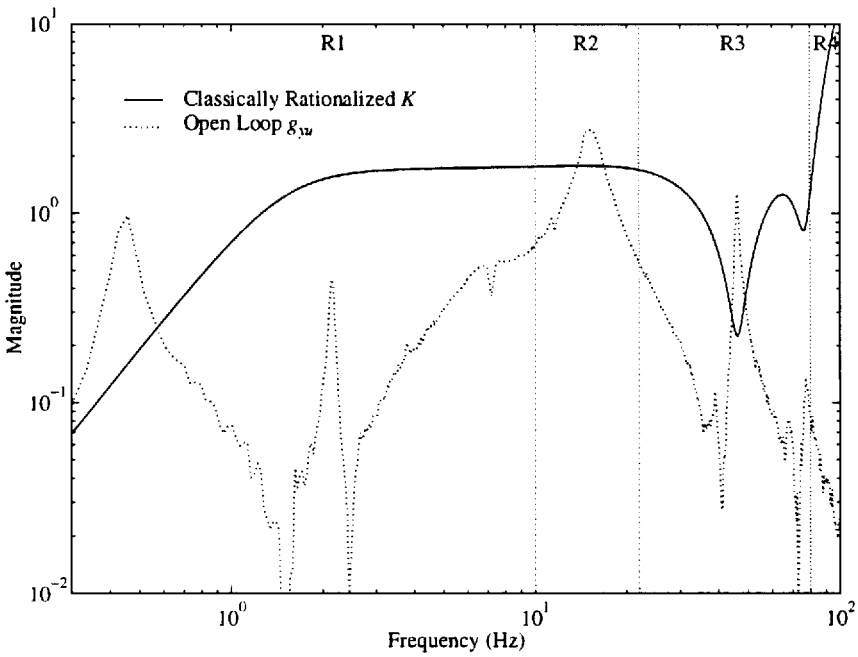

Fig. 8 Classically rationalized compensator for the nonanalogous MACE 1-*g* experiment.

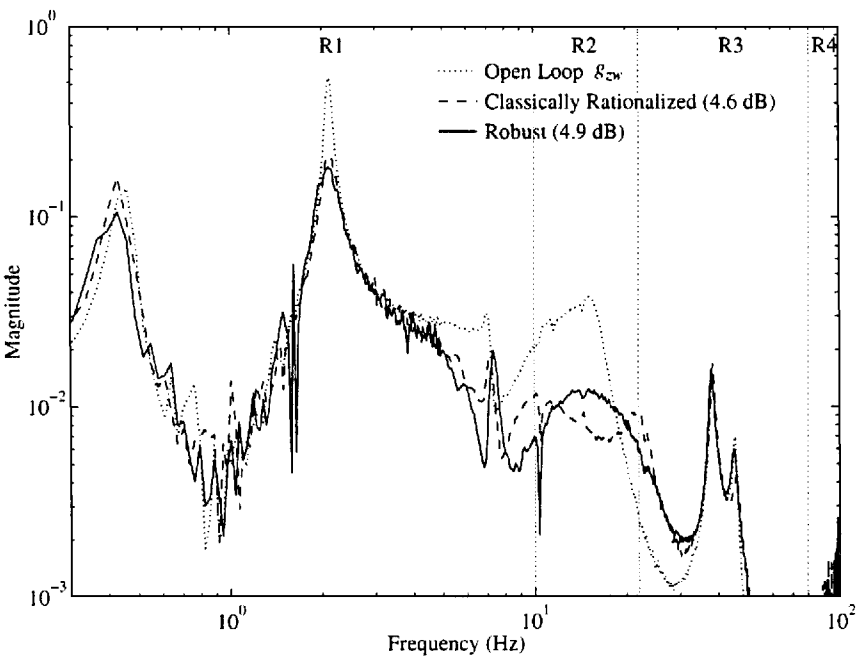

Fig. 9 Closed-loop disturbance to performance transfer functions for the nonanalogous MACE 1-*g* experiment.

A five-input, five-output classically rationalized controller was developed for this topology using the design rules in Sec. V. Table 4 gives a summary of the five loops in the order they were closed. The first three nonanalogous loops were designed similarly to the earlier example. The other two loops are output analogous problems and were designed differently.

Figure 10 shows the construction of the *Z*-axis output analogous controller (loop 5). Note that the input–output test is passed at all frequencies for this loop. Regions 3 and 4 are similar to the earlier example, using velocity feedback and notch filters in region 3 and a lead filter in region 4. The region 1 rule, however, matches the filter n_{zw}/n_{yu} using an integrator and lightly damped pole pair at 2.2 Hz. In region 2, the controller transitions to velocity feedback with no other dynamics. Loop 4 is designed similarly. It is noted that, even though loops 1–3 and 4 and 5 have similar bandwidths, an analysis of the 5 × 5 controller revealed no particular robustness or stability concerns.

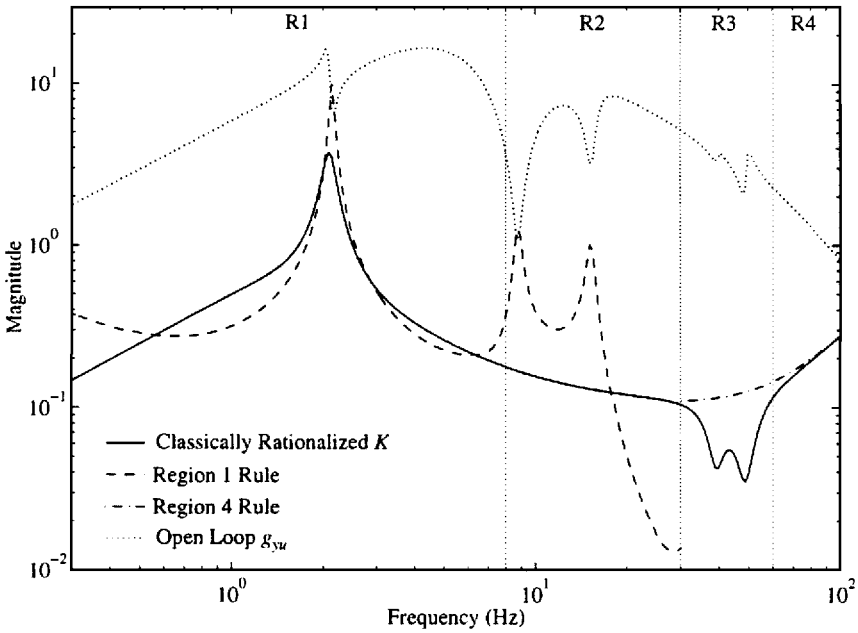

Fig. 10 Construction of the *Z*-axis output analogous portion of the classically rationalized controller for the MACE 0-*g* experiment.

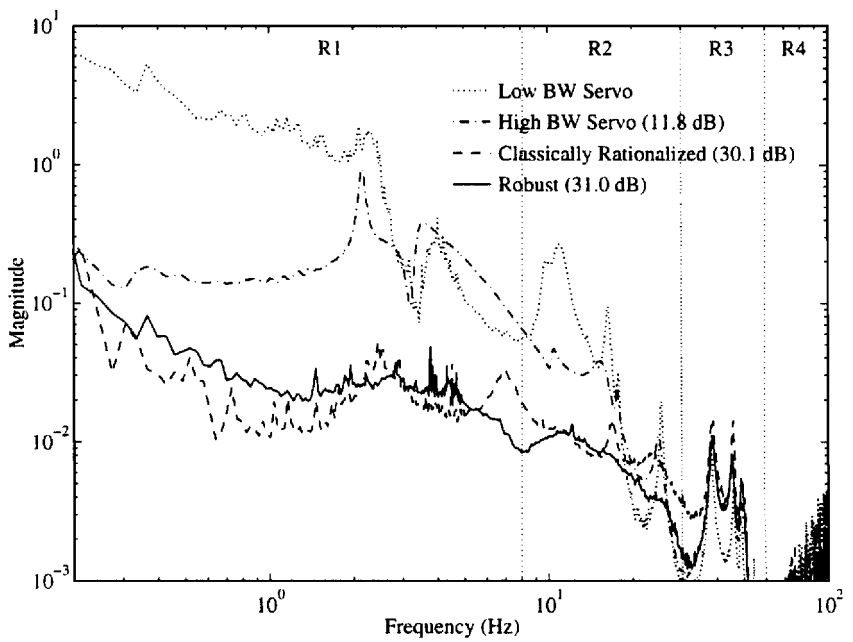

Fig. 11 Scalar closed-loop disturbance to performance transfer functions for the MACE 0-*g* experiment.

Figure 11 shows the measured closed-loop performance plots for the 40-state classically rationalized controller and the best robust control design from the mission, a 78-state multiple model controller. The performance metric is a combination of the *X* and *Z* integrated primary rate gyros. Low BW servo refers to the system with servos about each encoder-gimbal pair at one decade below the first flexible mode, whereas high BW servo refers to a servo with a bandwidth at the first flexible mode. The classically rationalized controller performed nearly as well as the robust design (30.1 vs 31.0 dB) with fewer states (40 vs 78). Both designs were limited by phase delay in the system.

The primary robust control design methodology for the MACE in 1 and 0 *g* is given in Refs. 4 and 18. After examining numerous methods, the SWLQG[4] and multiple model[1] methods were used because of their combination of good robustness, order, and design time properties. The classically rationalized design rules, however, have been used to design over 100 multivariable controllers in both 1 and 0 *g*. Overall, the classically rationalized controllers performed approximately as well as the SWLQG controllers and only slightly more poorly than the multiple model controllers, while using fewer states and design time. In addition, during the MACE mission, the rules were used to design over 50 closed-loop multivariable controllers on a variety of topologies, all of which were stable and performed quite well.

VII. Summary and Conclusions

This paper presents a detailed examination of LQG and frequency robust SWLQG controllers for four structural control topologies: fully analogous, output analogous, input analogous, and nonanalogous. Observations of how the optimal controllers compensate a structural mode in different frequency regions were summarized. The beneficial observations were then used to create a set of rules for the design of low-order, robust controllers. MIMO controllers can also be synthesized using a sequential loop closure method. The design rules were used to synthesize controllers for experimental implementation on the MACE in both 1 and 0 *g*, yielding quite good results for all types of systems including the most difficult nonanalogous and MIMO topologies.

Acknowledgments

This work was supported by the NASA IN-STEP Program and the NASA Langley Research Center Controlled Structures Interaction Office with Gregory Stover and Jerry Newsom as Contract Monitors.

References

[1]MacMartin, D. G., Hall, S. R., and Bernstein, D. S., "Fixed Order Multi-Model Estimation and Control," *Proceedings of the American Control Conference* (Boston, MA), Inst. of Electrical and Electronics Engineers, Piscataway, NJ, 1991, pp. 2113–2118.

[2]Collins, E. G., Jr., Phillips, D. J., and Hyland, D. C., "Robust Decentralized Control Laws for the ACES Structure," *Control Systems Magazine*, Vol. 11, April 1991, pp. 62–70.

[3]Balas, G. J., Young, P., and Doyle, J. C., "The Process of Control Design for the NASA Langley Minimast Structure," *Proceedings of the American Control Conference* (Boston, MA), Inst. of Electrical and Electronics Engineers, Piscataway, NJ, 1991, pp. 562–567.

[4]Grocott, S. C. O., How, J. P., and Miller, D. W., "Comparison of Control Techniques for Robust Performance on Uncertain Structural Systems," *Proceedings of the AIAA Guidance, Navigation, and Control Conference* (Scottsdale, AZ), AIAA, Washington, DC, 1994, pp. 261–271.

[5]Skelton, R. E., Hughes, P. C., and Hablani, H. B., "Order Reduction for Models of Space Structures Using Modal Cost Analysis," *Journal of Guidance, Control, and Dynamics*, Vol. 5, No. 4, 1982, pp. 351–357.

[6]Gregory, C. Z., Jr., "Reduction of Large Flexible Spacecraft Models Using Internal Balancing Theory," *Journal of Guidance, Control, and Dynamics*, Vol. 7, No. 6, 1984, pp. 725–732.

[7]Mercadal, M., "$\mathcal{H}_2$, Fixed Architecture, Control Design for Large Scale Systems," Ph.D. Thesis, Dept. of Aeronautics and Astronautics, Massachusetts Inst. of Technology, Cambridge, MA, June 1990.

[8]Wie, B., and Byun, K.-W., "New Generalized Structural Filtering Concept for Active Vibration Control Synthesis," *Journal of Guidance, Control, and Dynamics*, Vol. 12, No. 2, 1989, pp. 147–154.

[9]Wie, B., Horta, L., and Sulla, J., "Classical Control System Design and Experiment for the Mini-Mast Truss Structure," *Journal of Guidance, Control, and Dynamics*, Vol. 14, No. 4, 1991, pp. 778–784.

[10]Kwakernaak, H., and Sivan, R., *Linear Optimal Control Systems*, Wiley-Interscience, New York, 1972, Chap. 5.

[11]Sesak, J. R., "Sensitivity Constrained Linear Optimal Control Analysis and Synthesis," Ph.D. Thesis, Univ. of Wisconsin, Madison, WI, 1974.

[12]Yedevalli, R. K., and Skelton, R. E., "Controller Design for Parameter Sensitivity Reduction in Linear Regulators," *Optimal Control Applications and Methods*, Vol. 3, No. 3, 1982, pp. 221–240.

[13]Miller, D. W., How, J. P., Campbell, M. E., Grocott, S., Liu, K., Glaese, R. M., and Tuttle, T., "Flight Results from the Middeck Active Control Experiment (MACE)," *AIAA Journal*, Vol. 36, No. 3, 1998, pp. 432–440.

[14]Miller, D. W., Crawley, E. F., How, J. P., Liu, K., Campbell, M. E., Grocott, S. C. O., Glaese, R. M., and Tuttle, T. D., "The Middeck Active Control Experiment (MACE): Summary Report," Space Engineering Research Center, SERC 7-96, Massachusetts Inst. of Technology, Cambridge, MA, June 1996.

[15]Campbell, M. E., and Crawley, E. F., "Asymptotic Linear Quadratic Control for Lightly Damped Structures," *Journal of Guidance, Control, and Dynamics*, Vol. 19, No. 4, 1996, pp. 969–971.

[16]Gevartner, W. B., "Basic Relations of Flexible Vehicle," *AIAA Journal*, Vol. 8, No. 4, 1970, pp. 666–672.

[17]Glaese, R. M., and Miller, D. W., "Derivation of Zero-Gravity Structural Control Models from Analysis and Ground Experimentation," *Journal of Guidance, Control, and Dynamics*, Vol. 19, No. 4, 1996, pp. 787–793.

[18]Campbell, M. E., Grocott, S. C. O., and How, J. P., "Overview of Closed Loop Results for MACE," *Proceedings of the IFAC 13th World Congress*, Vol. D, Elsevier Science, Oxford, England, UK, 1996, pp. 49–54.